Large scale changes in 20th Century black carbon deposition to Antarctica

Marion M. Bisiaux[1*], Ross Edwards[2], Joseph R. McConnell[1], Mark A. J. Curran[3,4], Tas D. Van Ommen[3,4], Andrew M. Smith[5], Thomas A. Neumann[6], Daniel R. Pasteris[1], Joyce E. Penner[7] and Kendrick Taylor[1].

[1] Desert Research Institute, Reno, NV, United States,

[2] Curtin University of Technology, Bentley, WA, Australia

[3] Australian Antarctic Division, Kingston, TAS, Australia,

[4] Antarctic Climate and Environment CRC, University of Tasmania, Hobart, TAS, Australia,

[5] Australian Nuclear Science and Technology Organisation, Lucas Heights, NSW, Australia,

[6] Goddard Space Flight Center, NASA, Greenbelt, MD USA,

[7] University Michigan, Ann Arbor, MI, United states

*Correspondence to: M. M. Bisiaux (marion.bisiaux@dri.edu)

Black carbon measurements

Continuous flow analysis was based on a steady sample flow and in-line detection of BC and other chemical substances as described in McConnell et al. (2007). In the cold room, previously cut one meter ice core sticks of 3x3cm, are melted continuously on a heated melter head specifically designed to eliminate contamination from the atmosphere or by the external parts of the ice. The melted ice from the most inner part of the ice stick is continuously pumped by a peristaltic pump and carried to a clean lab by Teflon lines. The recorded signal is continuous, integrating a sample volume of about 0.05 mL, for which the temporal resolution depends on the speed of melting, ice density and snow accumulation rate at the ice core drilling site. The two ice cores presented in this study have monthly to seasonal resolution over the time period that was examined.

Refractory black carbon (rBC) concentrations were determined using the same method as in (Bisiaux et al., 2011) and adapted to continuous flow measurements as described by (McConnell et al., 2007). The technique uses a single particle intracavity laser induced incandescence photometer (SP2, Droplet Measurement Technologies, Boulder, Colorado) coupled to an ultrasonic nebulizer/desolvation (CETAC UT5000) Flow Injection Analysis (FIA). All analyses, sample preparation etc, were performed in a class 100 cleanroom using anti contamination "clean techniques". The samples were not acidified.

Calibration of the incandescence intensity was performed by introducing size-selected rBC nanoparticles (graphite particles of known density) into the SP2 using a differential mobility analyzer (DMA, performed by Droplet Measurement Technologies) (Slowik et al., 2007). Previous studies have found that the SP2 response is independent of rBC particle morphology (Cross et al., 2010), rBC coatings (Moteki and Kondo, 2007) and that the DMA calibration using graphitic rBC is applicable to rBC nanoparticles emitted by combustion (Schwarz et al., 2010).

External calibration of the nebulizer/SP2 interface was performed using pure, commercial rBC dispersions (Tokai Carbon, Aquablack 162) with a similar surface chemistry to that of hydrophilic rBC aerosols found in the atmosphere (Moosmüller et al., 2009). The instrumental response of these standards ($0.03x10^{-3}$ to $40x10^{-3}$ µg/L with 9 standards) was compared with a hydrophilic rBC dispersion produced by an inverted diffusion flame and ozonation (Kirchstetter and Novakov, 2007) and were found to give a comparable response. The commercial rBC was also used to prepare quality control standards, which were determined along with blanks every ~2 hours of continuous melting. Blanks were found below the method detection limit (~ $0.01x10^{-3}$ µg/L, 3σ). rBC concentrations were quantified by first calculating the individual rBC masses using the DMA incandescence calibration and then summing the rBC masses over three second intervals (3 sec). The FIA peaks in the resulting 3 sec mass time series were integrated and the peak areas was used to construct an external linear calibration, which was subsequently used to quantify the sample peak areas. Thus, interpolation below the detection limit is not performed as in Kaspari 2011. However, variability due to different calibration methods may not influence the relative changes observed in the records presented here and which are interpreted qualitatively. Indeed, ice core

replicates analyzed at the beginning of each experimental day were found very reproducible with standard deviation lower than ~10%.

Dating

The cores were dated by counting the annual cycles in trace chemistry notably in Sodium (Na), Chlorine (Cl), Sulfur (S) and Bromine (Br). Annual layer counting was evaluated using cross comparisons of peaks in S concentration in the DSS0506 collected from the high snow accumulation region at the top of Law Dome for specific volcanic horizons including Tambora (1815), and Krakatoa (1883) and Agung (1963).

For annual accumulation derived from the ice cores, we assumed ~3.1 cm water equivalent uncertainty in each year's accumulation from short scale spatial variability (glaciological noise) which was determined from measurements of annual accumulation in multiple parallel ice cores from the WAIS Divide ice core site (Banta et al., 2008).

Fluxes

Annual rBC flux rates were calculated at WAIS by summing monthly flux rates (estimated by dividing the annual accumulation rate by 12 and multiplying by the monthly concentrations). A model estimate of the measured annual layer thinning due to ice flow proved to be very minimal in the most recent 150 years (measured layer thickness is ~1% less than the initial layer thickness) so no correction was made to the accumulation rates derived from the WDC06A ice core.

While the ice cores reflect sub-seasonal variations at both LD and WAIS, the measurements at LD lack unambiguous subannual markers that can be tied to specific calendar dates and for this reason only the annual averages in accumulation were derived from the record (mid-January to mid-January) (van Ommen and Morgan, 2010).

Spectral analysis

To investigate and extract the most prominent frequencies of our signal, we conducted spectral analysis on the rBC and Na records with Kspectra 3.0.2.software for multitaper method (Ghil et al., 2002) and with Analyseries 2.0.3 software (Paillard, 1996) for Blackman-Tukey method (coherence and phasing) on Macintosh. We used different spectral analysis and compared them to confirm the robustness of our results.

Resampling, smoothing and spectral analysis were conducted on the log of the original values, then changed back to normal.

Multitaper method (MTM), Figure 3 and SI-4:

This method is independent of the spectral power, and even small amplitude oscillations may be considered as significant. This is not the case with a Blackman-Tukey method. The significance of each spectral peak is determined through a F-test (>0.90, >0.95, >0.99). We used monthly resolution record for this analysis. In our cases, with monthly resolution over 150 years, we use a number of tapers of 3, and resolution = 2. For typical length instrumental climate records, this offers a good compromise between the required frequency resolution for resolving distinct climate signals (e.g., ENSO and decadal-scale variability) and the benefit of multiple spectral degrees of freedom (http://www.spectraworks.com/Help/). We used in particular the high-resolution multitaper spectrum which is the weighted sum of the K eigenspectra, with a red noise significance (robust noise), reshaped at 95% with linear fit.

Blackman-Tukey method (Figure SI-3 and SI-5)

This is the classical method for spectral analysis. In particular, we used it to determine the phase relationship between two data sets (between two sites or between rBC and Na), using two different filters to get the best spectral coherence for any given frequency. This coherence is a function of frequency with values between 0 and 1, and is a fraction of a common variance between two time series x and y through a linear relation. Coherence coefficients are given with 3 levels of confidence (high, medium levels -shown on graph- and low). Coherence is considered non-zero when coefficients reach for values > 0.38.

For this analysis we resampled (using piece-wise linear integration interpolation) the different datasets, using a time resolution 0.4 yrs, to keep the annual periodicity but remove any shorter-term variability. Phasing between the same periodicities was also determined through this method, and is given as a positive or negative value in radians as a function of delay between the two series.

Variance estimation

For variance calculation, we used this following equation:

$$\frac{\sum (x-\bar{x})^2}{n}$$

where x is the average of the data set (in log, thus the geometric mean) and n is the size of the data set. To represent the period of low variance (Fig. SI-6) we choose to apply a 21months running variance to the data set.

Supplemental information references

Banta, J. R., McConnell, J. R., Frey, M. M., Bales, R. C., and Taylor, K.: Spatial and temporal variability in snow accumulation at the West Antarctic Ice Sheet Divide over recent centuries, Journal of Geophysical Research, 113, D23102, 10.1029/2008jd010235, 2008.

Bisiaux, M. M., Edwards, R., Heyvaert, A. C., Thomas, J. M., Fitzgerald, B., Susfalk, R. B., Schladow, S. G., and Thaw, M.: Stormwater and fire as sources of black carbon nanoparticles to Lake Tahoe, Environ Sci Technol, 45, 2065-2071, 10.1021/es103819v, 2011.

Cross, E. S., Onasch, T. B., Ahern, A., Wrobel, W., Slowik, J. G., Olfert, J., Lack, D. A., Massoli, P., Cappa, C. D., Schwarz, J. P., Spackman, J. R., Fahey, D. W., Sedlacek, A., Trimborn, A., Jayne, J. T., Freedman, A., Williams, L. R., Ng, N. L., Mazzoleni, C., Dubey, M., Brem, B., Kok, G., Subramanian, R., Freitag, S., Clarke, A., Thornhill, D., Marr, L. C., Kolb, C. E., Worsnop, D. R., and Davidovits, P.: Soot Particle Studies--Instrument Inter-Comparison--Project Overview, Aerosol Science and Technology, 44, 592 - 611, 2010.

Ghil, M., Allen, M. R., Dettinger, M. D., Ide, K., Kondrashov, D., Mann, M. E., Robertson, A. W., Saunders, A., Tian, Y., Varadi, F., and Yiou, P.: Advanced spectral methods for climatic time series, Review of Geophysics, 40, 1003, 10.1029/2000rg000092, 2002.

Kirchstetter, T. W., and Novakov, T.: Controlled generation of black carbon particles from a diffusion flame and applications in evaluating black carbon measurement methods, Atmos Environ, 41, 1874-1888, 2007.

McConnell, J. R., Edwards, R., Kok, G. L., Flanner, M. G., Zender, C. S., Saltzman, E. S., Banta, J. R., Pasteris, D. R., Carter, M. M., and Kahl, J. D. W.: 20th-century industrial black carbon emissions altered arctic climate forcing, Science, 317, 1381-1384, 10.1126/science.1144856, 2007.

Moosmüller, H., Chakrabarty, R. K., and Arnott, W. P.: Aerosol light absorption and its measurement: A review, Journal of Quantitative Spectroscopy and Radiative Transfer, 110, 844-878, 2009.

Moteki, N., and Kondo, Y.: Effects of mixing state on black carbon measurements by laser-induced incandescence, Aerosol Science and Technology, 41, 398-417, 2007.

Paillard, D., L. Labeyrie, and P. Yiou: Macintosh program performs time-series analysis, Eos Trans. AGU, 77, 379, 1996.

Schwarz, J. P., Spackman, J. R., Gao, R. S., Perring, A. E., Cross, E., Onasch, T. B., Ahern, A., Wrobel, W., Davidovits, P., Olfert, J., Dubey, M. K., Mazzoleni, C., and Fahey, D. W.: The Detection Efficiency of the Single Particle Soot Photometer, Aerosol Science and Technology, 44, 612-628, 2010.

Slowik, J. G., Cross, E. S., Han, J. H., Davidovits, P., Onasch, T. B., Jayne, J. T., WilliamS, L. R., Canagaratna, M. R., Worsnop, D. R., Chakrabarty, R. K., Moosmuller, H., Arnott, W. P., Schwarz, J. P., Gao, R. S., Fahey, D. W., Kok, G. L., and Petzold, A.: An inter-comparison of instruments measuring black carbon content of soot particles, Aerosol Science and Technology, 41, 295-314, 10.1080/02786820701197078, 2007.

van Ommen, T. D., and Morgan, V.: Snowfall increase in coastal East Antarctica linked with southwest Western Australian drought, Nat Geosci, 3, 267-272, 2010.

Figure captions

-Figure SI-1: 1970-2000 monthly (dots) and annual smoothing (line) for Na at WAIS and Law Dome.

-Figure SI-2: Distribution of rBC (left) and Na (right) data points at WAIS (top) and Law Dome (bottom) (black dots) and corresponding modeled log-normal fit, for 1850-2001 and 1970-2001.

-Figure SI-3: Top. Average (thick) and max-min (thin) coherence coefficients for 1970-2001 period between rBC and Na records for WAIS(a) and LD(c). Non zero coherence is > 0.38 and shaded. Time resolution is 0.4yr (Blackman Tukey spectrum using Bartlett window, bandwidth 0.098).
Bottom: Phasing between rBC and Na periodicities in radians for WAIS(b) and LD(d). Na leads for values >0. ENSO bands (~0.15-3 cycle/yr or ~3-7 years) and 1-yr bands are shown as dash lines. Black numbers indicate delay between rBC and Na in years at those corresponding periodicities.

Figure SI-4: Spectrum obtained with Multi Taper Method for WAIS (a) and LD (b) monthly Na records for 1850-2001 period and confidence levels in red lines (90, 95, 99%). Numbers on graph indicate significant periodicities in years.

Figure SI-5: Average coherence (thick) and max/min (thin) between LD and WAIS periodicities for rBC (a) and Na (b) for the 1970-2001 period at a 0.4yr time resolution (Blackman Tukey spectrum using a Bartlett window, bandwidth 0.098, non-zero coherence >0.38). ENSO bands (~0.15-3 cycle/yr or ~3-7 years) and 1-yr bands are shown as dash lines.

Figure SI-6: moving variance (on log values) calculated for 21 months, from 1850 to 2000 at WAIS (a, c) and LD (b, d), for rBC (a, b) and Na (c, d). A period of low variance from 1955 to 1985 is common to the two sites, but only in rBC record.

Figure SI-1

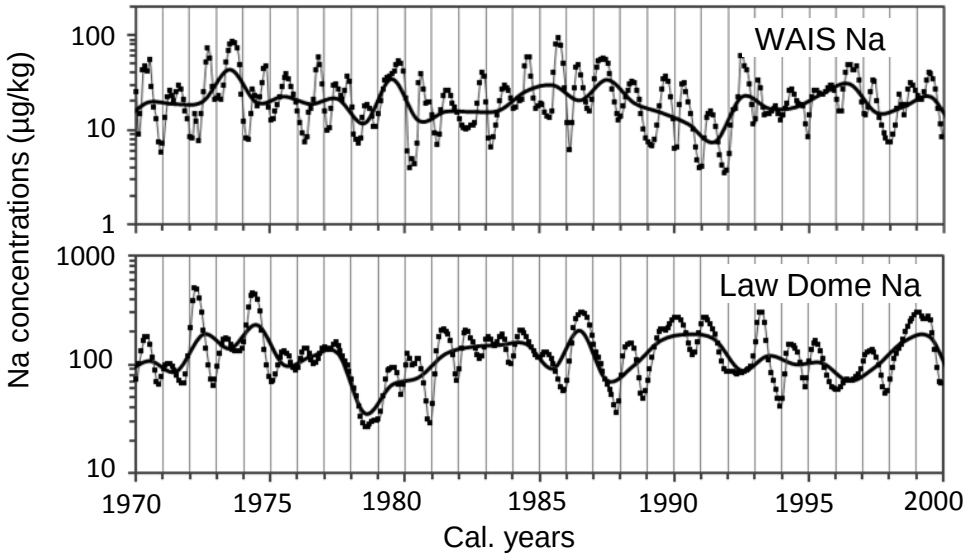
WAIS Na
Law Dome Na
Na concentrations (µg/kg)
100
10
1
1000
100
10
1970
1975
1980
1985
1990
1995
2000
Cal. years

Figure SI-2

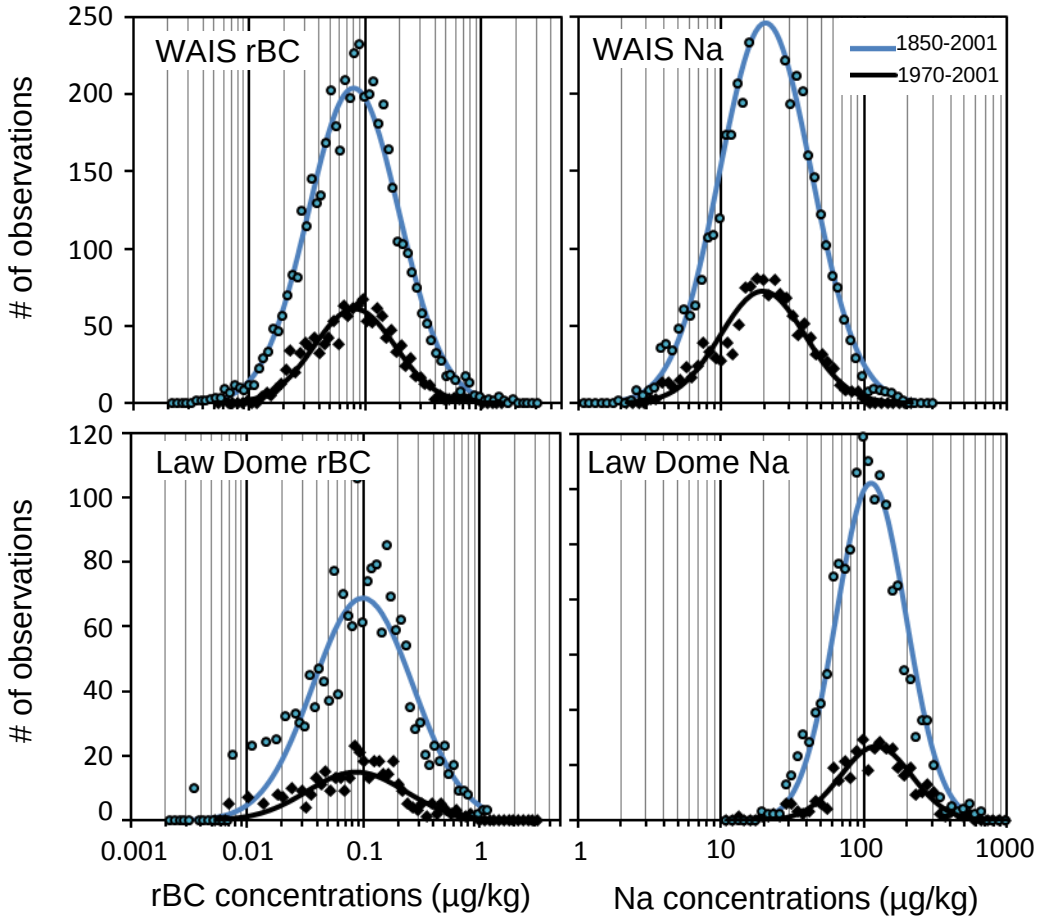
WAIS rBC
WAIS Na
1850-2001
1970-2001
Law Dome rBC
Law Dome Na
# of observations
# of observations
250
200
150
100
50
0
120
100
80
60
40
20
0
0.001
0.01
0.1
1
1
10
100
1000
rBC concentrations (µg/kg)
Na concentrations (µg/kg)

Figure SI-3

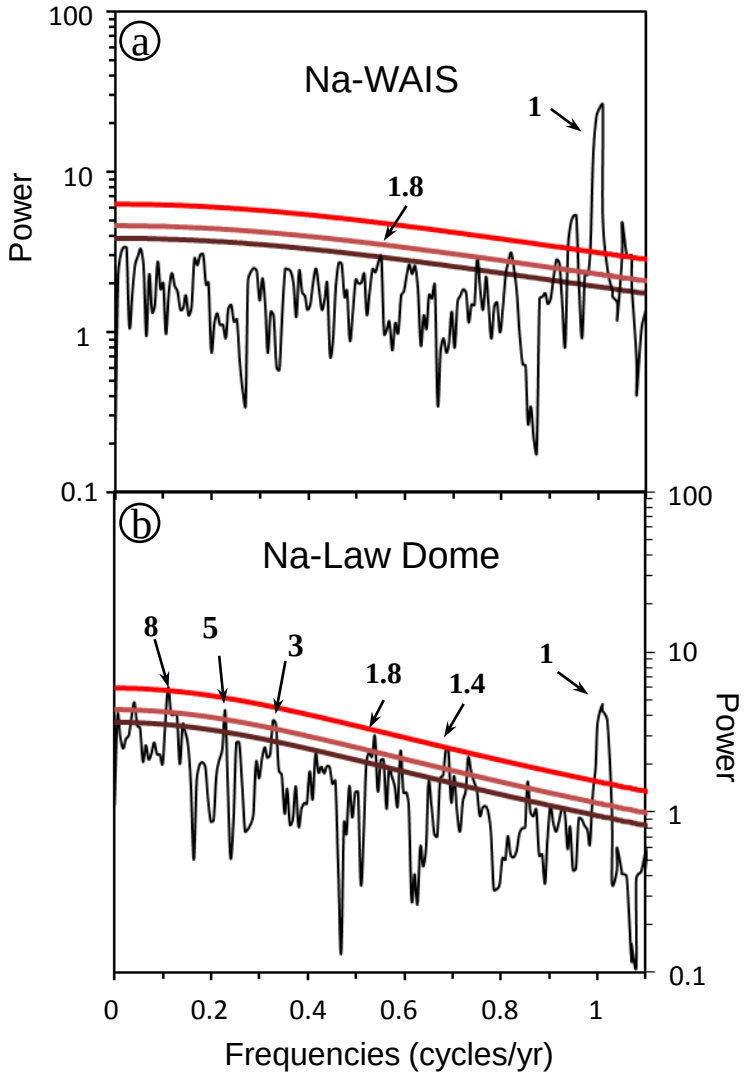
a
Na-WAIS
1
1.8
b
Na-Law Dome
8
5
3
1.8
1.4
1
Power
100
10
1
0.1
0
0.2
0.4
0.6
0.8
1
Frequencies (cycles/yr)

Figure SI-4

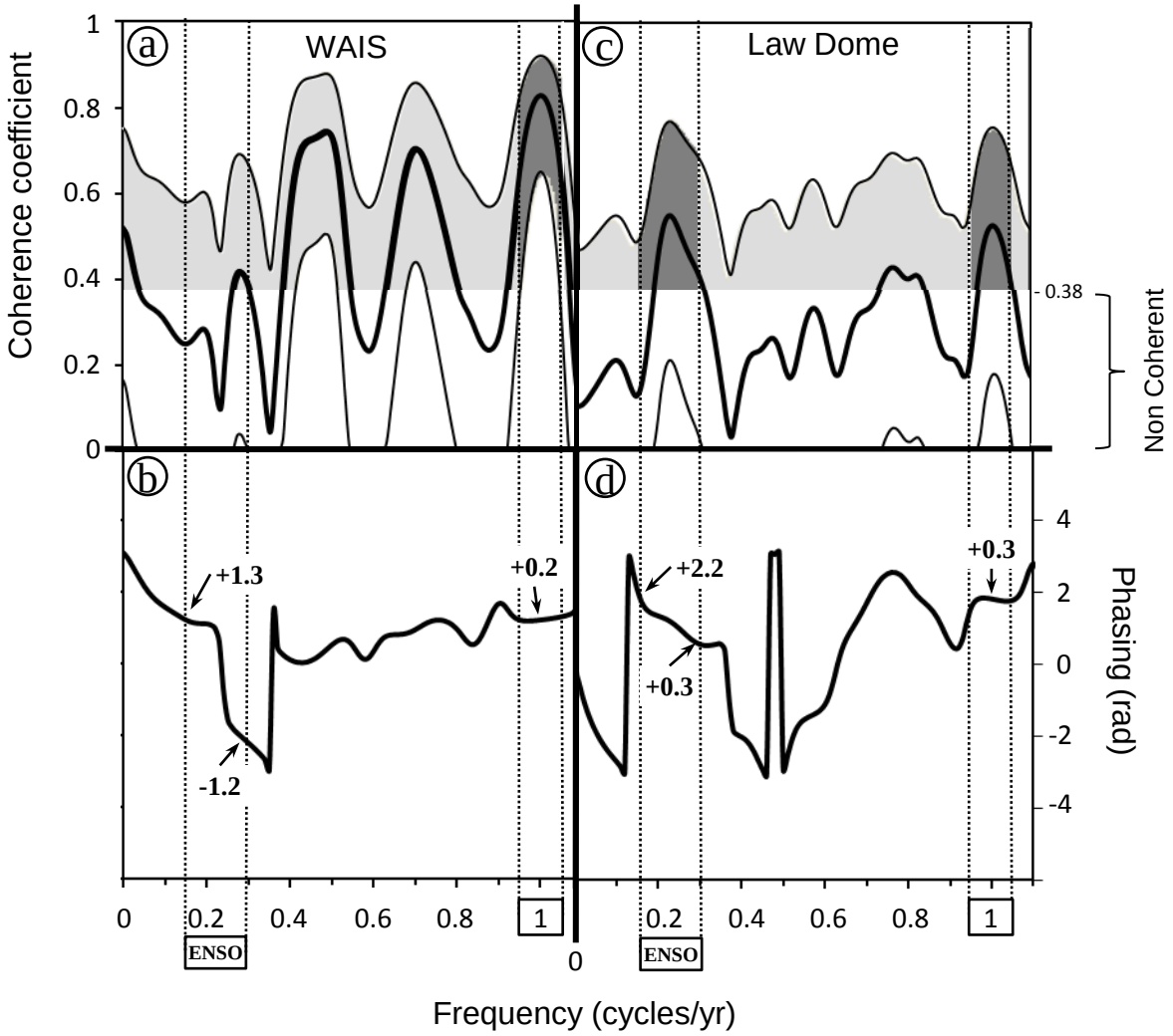
a
WAIS
c
Law Dome
Coherence coefficient
1
0.8
0.6
0.4
0.2
0
0.38
Non Coherent
b
d
+1.3
-1.2
+0.2
+2.2
+0.3
+0.3
4
2
0
-2
-4
Phasing (rad)
0
0.2
0.4
0.6
0.8
1
ENSO
0
0.2
0.4
0.6
0.8
1
ENSO
Frequency (cycles/yr)

Figure SI-5

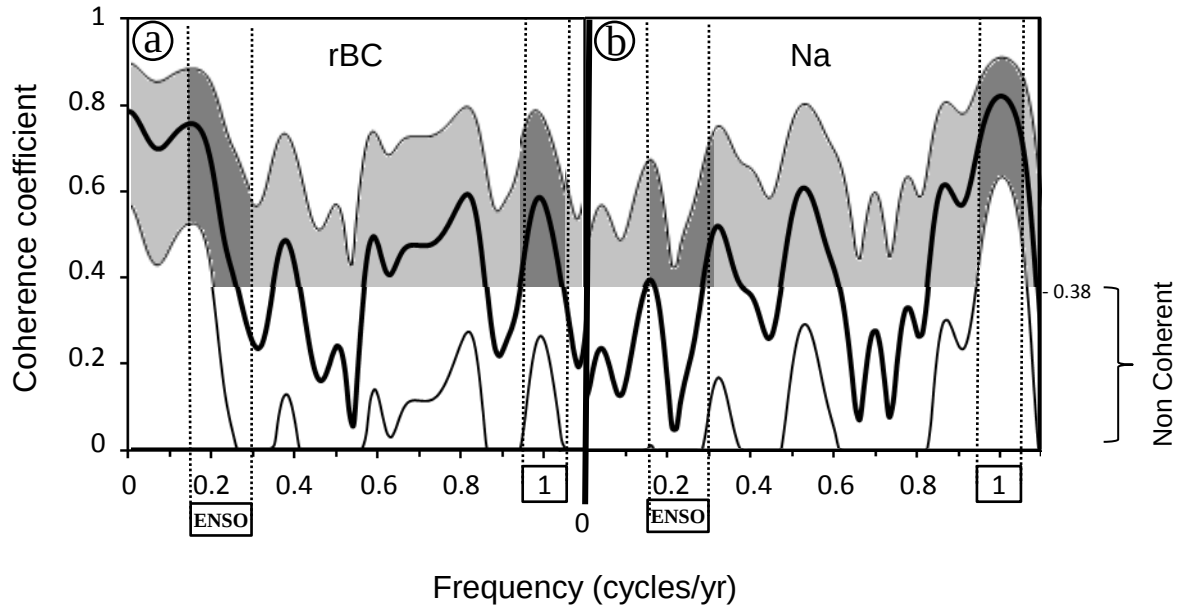
a
rBC
b
Na
Coherence coefficient
1
0.8
0.6
0.4
0.2
0
0.38
Non Coherent
0
0.2
0.4
0.6
0.8
1
ENSO
Frequency (cycles/yr)

Figure SI-6

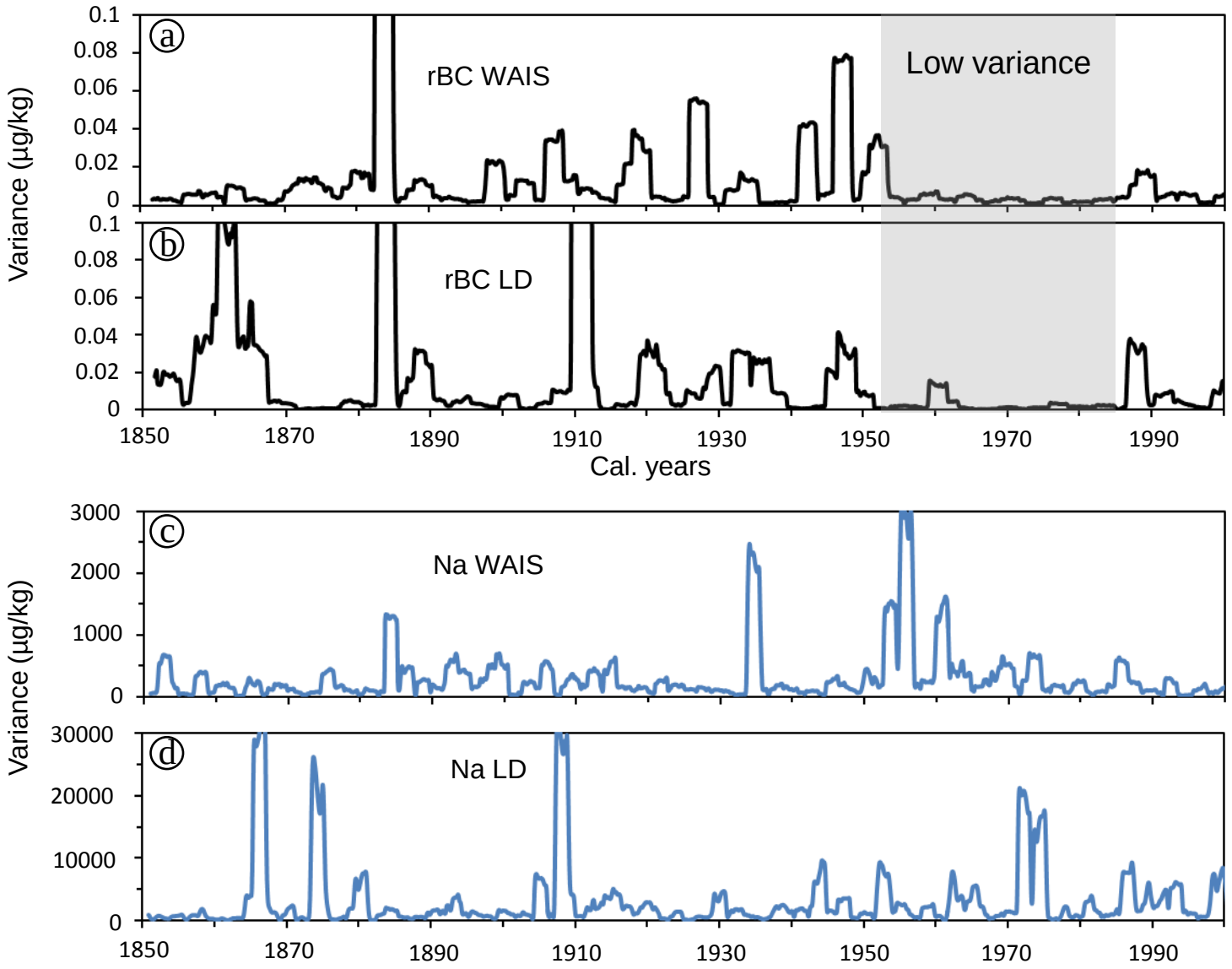
a
rBC WAIS
Low variance
b
rBC LD
Variance (µg/kg)
0.1
0.08
0.06
0.04
0.02
0
1850
1870
1890
1910
1930
1950
1970
1990
Cal. years
c
Na WAIS
d
Na LD
3000
2000
1000
30000
20000
10000